metals

MDPI

Article

High Temperature Oxidation and Wear Behaviors of Ti–V–Cr Fireproof Titanium Alloy

Guangbao Mi [1], Kai Yao [2], Pengfei Bai [2], Congqian Cheng [2] and Xiaohua Min [2,*]

[1] Key Laboratory of Science and Technology on Advanced Titanium Alloys, AECC Beijing Institute of Aeronautical Materials, Beijing 100095, China; miguangbao@163.com

[2] School of Materials Science and Engineering, Dalian University of Technology, Dalian 116024, China; kaiyao@mail.dlut.edu.cn (K.Y.); bpf2014@mail.dlut.edu.cn (P.B.); cqcheng@dlut.edu.cn (C.C.)

* Correspondence: minxiaohua@dlut.edu.cn; Tel.: +86-411-8470-8189

Received: 26 April 2017; Accepted: 14 June 2017; Published: 19 June 2017

Abstract: The high temperature oxidation and wear behaviors of Ti–35V–15Cr–0.3Si–0.1C fireproof titanium alloy were examined at 873 and 1073 K. The oxidation weight gain after oxidation at 1073 K for 100 h was significantly larger than that at 873 K. Based on the analyses of the oxidation reaction index and oxide layer, the oxidation process at 1073 K was mainly controlled by oxidation reaction at the interface between the substrate and oxide layer. Dry sliding wear tests were performed on a pin-on-disk tester in air conditions. The friction coefficient was smaller at 1073 K than that at 873 K, while the volume wear rate at 1073 K was larger due to formation of amount of oxides on the worn surface. When the wearing temperature increased from 873 to 1073 K, the wear mechanism underwent a transition from a combination of abrasive wear and oxidative wear to only oxidative wear.

Keywords: titanium alloy; fireproof; oxidation; high temperature wear; mechanism

1. Introduction

Titanium and its alloys are widely used in aerospace, chemical, and biomedical industries because of high specific strength and excellent corrosion resistance, especially for their applications in aero-engines [1–3]. However, conventional titanium alloys can be ignited and burned, known as "titanium fire," under specific conditions of high temperature, high pressure, and high-speed airflow, which limits their application for advanced aero-engines [4–6]. With the improvement of the thrust-weight ratio, the work conditions of components such as the case, blade, and disk becomes more complex and severe, resulting in an increase in the occurrence of titanium fire. Compared with other techniques including structural optimization design, surface alloying, and surface coating, the development of advanced fireproof titanium alloys is more desirable to completely prevent the occurrence of titanium fire in aero-engines, as well as to meet its high thrust-weight ratio [4,7].

Titanium fire is known to a typical accident of igniting, which occurs usually through high-energy friction and load impact as an ignition source, for example, between the blade and case. The whole combustion behavior goes through high temperature oxidation, super high temperature oxidation, burning, self-sustained combustion, and burning out [4]. If titanium alloys are ignited, the components in the compressor burn continually only for 4–20 s under gas flow with high temperature and pressure. The burning time is too short to take extinguishing measures. There are two types of fireproof titanium alloys: Ti–V–Cr base alloys, such as Ti–35V–15Cr (Alloy C), Ti–35V–15Cr–0.6Si–0.05C (Alloy C$^+$), Ti–25V–15Cr–2Al–0.2C, Ti–25V–15Cr–0.2Si (Ti40), and Ti–35V–15Cr–0.3Si–0.1C (TF550) alloys [8–11]; and Ti–Cu–Al base alloys, such as Ti–13Cu–4Al–4Mo–2Zr (BTT–1), Ti–18Cu–2Al–2Mo (BTT–3), and Ti–13Cu–1Al–0.2Si (Ti14) [12–14]. Note that abovementioned and other compositions in this study are expressed in mass%. Ti–V–Cr base alloys are highly stabilized β-type titanium alloys with better performance than that of Ti–Cu–Al base alloys.

In case of TF550 fireproof titanium alloy, we previously investigated the fireproof behavior by the frictional ignition method, and found that the presence of oxides on the worn surface such as TiO_2, V_2O_5, and Cr_2O_3 affected the lubrication behavior in the local area of friction [15–17]. However, the high temperature oxidation and wear behaviors remain unclear for this alloy, which are considered to be closely associated with their fireproof properties. The shortage of studies results in uncertainty of the fireproof level of titanium alloys used in aero-engines and restricts the material selection of fireproof titanium alloys for engine designers. Thus, the purpose of present study is to examine the oxidation and wear behaviors of TF550 alloy at high temperatures of 873 and 1073 K, and to discuss the mechanisms of high temperature oxidation and wear.

2. Experimental Procedures

2.1. Materials Preparation

An ingot of approximately 150 kg of TF550 alloy was fabricated by consumable vacuum arc melting (ZHT-650, Baoji institute of rare metal research, Baoji, China) with the raw materials of titanium sponge, pure vanadium rods, and chromium sponge. Subsequently, it was subjected to sheathed extrusion, forging and rolling, and its actual composition was Ti–35.5V–14.6Cr–0.32Si–0.11C. For oxidation testing, samples with a dimension of 12 mm (l) × 10 mm (w) × 6 mm (t) were cut from the rolled plate and their surfaces were mechanically polished with SiC abrasive paper in order to evaluate their high temperature oxidation behavior. As-received Ti–6Al–4V alloy was used to evaluate the oxidation behavior as a comparison. For wear testing, pins and disks were also cut from the rolled plate (HQ1UP, Hanqi Company, Suzhou, China). The rod as pins was designed in the form of a cylinder with a diameter of 5 mm and a height of 9 mm, and the contact surface was a half-ball with a diameter of 5 mm. Disks with the dimensions of 25 mm diameter and 10 mm thickness were used. The contact surfaces of pins and disks were mechanically polished (UNIPOL-1200M, Kejing Company, Shenyang, China) with SiC abrasive paper and then cleaned in alcohol.

2.2. Oxidation Testing

Before oxidation testing, the samples and crucibles were ultrasonically cleaned (XY-CS-S, Xinyi Company, Shanghai, China) in alcohol. In addition, the crucibles were baked at 1373 K for 20 h to ensure their constant weight during the whole oxidation process. Oxidation tests were carried out at 873 and 1073 K for a total oxidation time of 100 h. During the oxidation period, they were cooled down to room temperature at an interval of 10 h in order to measure their weight and observe their surface morphology. Oxidation kinetics were examined based on the weight gain per unit area versus oxidation time.

2.3. Wear Testing

Dry sliding wear tests were performed on a pin-on-disk tester (THT-04015, CSM Company, Carouge, Switzerland) in air conditions at temperatures of 873 and 1073 K. A pin was loaded against a rotating disk through the mechanical loading system with a normal load of 4.9 N for 30 min. The sliding velocity was 0.2 m/s along a diameter of 10 mm circular path with total sliding distance of 3.6×10^2 m, which was proved to be sufficient to attain a steady-state condition [18–21]. The friction coefficient was recorded by the tester automatically, and the mean friction coefficient was calculated based on the whole data, which was recorded during the sliding wear tests. Volume wear rate was calculated as follows:

$$Ws = \Delta V / (PL) \quad (1)$$

where ΔV, P, and L are the volume loss of disk, applied loading and sliding distance, respectively. For the disk, four different regions of the wearing indent were measured by using nanomap-3D microscopy (AEP Company, Columbus, OH, USA) for 3D micrograph and the corresponding cross-section area of the wearing indent, and then the volume loss was obtained by the mean

cross-section area multiplied by the circumference of the wearing indent. For the pin, the volume loss was obtained by the wearing volume of the half-ball of pin.

2.4. Microstructural Characterization

Phase identification was made by X-ray diffraction analysis (XRD) using an EMPYREN diffractometer with Cu-Kα radiation operated at 40 kV and 300 mA (Panalytical, Almelo, The Netherlands). Morphologies including backscattered electron image (BEI) and secondary electron image (SEI), and chemical compositions were examined by a SUPRA55 type scanning electron microscope (SEM, Carl Zeiss Jena Company, Oberkochen, Germany) equipped with an energy dispersive spectrometer (EDS).

3. Results and Discussion

Figure 1 shows the oxidation kinetics curves of TF550 alloy along with Ti–6Al–4V alloy after oxidation at 873 and 1073 K for 100 h. As shown in Figure 1a, with increasing oxidation time, the oxidation weight gain of each alloy showed an increase tendency, and it was much larger at 1073 K than that at 873 K. The oxidation weight gain of TF550 alloy was 2 mg/cm^2 after oxidation at 873 K for 100 h, which was similar with that (1.4 mg/cm^2) of Ti–6Al–4V alloy, while the oxidation weight gain of TF550 alloy (90 mg/cm^2) was larger than that (40 mg/cm^2) of Ti–6Al–4V alloy at 1073 K. The smaller oxidation weight gain of Ti–6Al–4V alloy was attributed to the formation of the compact Al_2O_3 layer, which could prevent the further oxidation of the substrate [22,23]. Although the oxidation weight gain of Ti–6Al–4V alloy was smaller than that of TF550 alloy, the oxide layer of Ti–6Al–4V alloy flaked seriously at 1073 K, as shown in Figure 2a. While V_2O_5 which formed in the oxide layer of TF550 alloy, it melted and flowed into the crucible (yellow matters in Figure 2b) due to its low melting point (about 948 K) [24,25]. The formation of V_2O_5 in TF550 alloy at high temperatures improved the wear properties resulting from their lubrication, which could enhance its burn-resistant behavior. The detailed discussion is shown in Section 3.

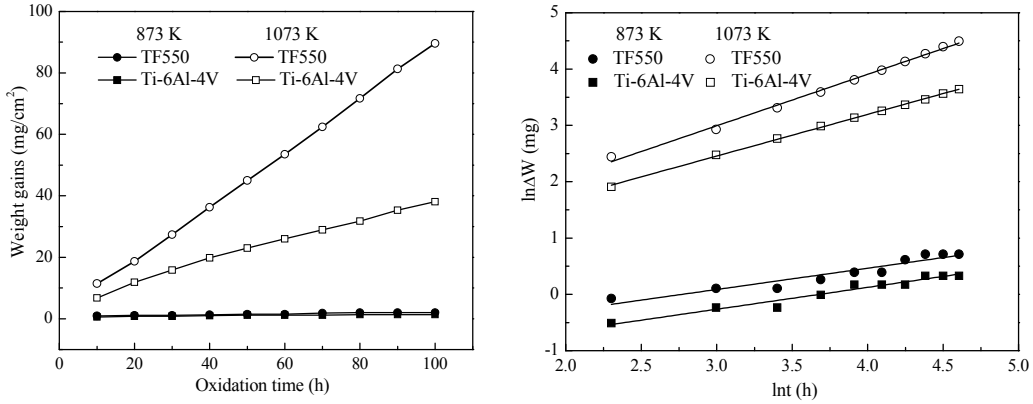

Figure 1. Oxidation kinetics curves of TF550 alloy along with Ti–6Al–4V alloy at temperatures of 873 and 1073 K. (**a**) Oxidation weight gain curves and (**b**) double logarithmic curves.

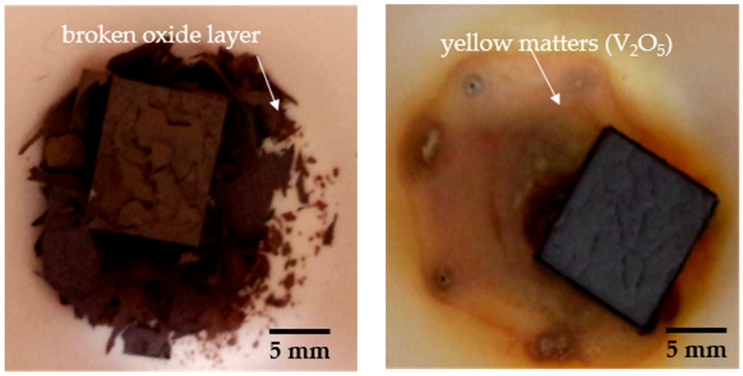

Figure 2. Macroscopic morphologies of TF550 alloy along with Ti–6Al–4V alloy after oxidation at 1073 K for 100 h. (**a**) Ti–6Al–4V and (**b**) TF550.

Figure 3 shows the X-ray diffraction profiles of TF550 alloy at 873 and 1073 K for 100 h. The surface oxide product was identified as TiO_2 and V_2O_5 at 873 K, while it was detected to be only TiO_2 at 1073 K. In addition, the peak intensity of V_2O_5 was weaker than that of TiO_2 at 873 K. Based on the oxidation kinetic relationship [26],

$$\Delta W = kt^n \tag{2}$$

where ΔW is the oxidation weight gain, n is the oxidation reaction index and t is the oxidation time, respectively. The oxidation reaction index (n) could be obtained to discuss the oxidation mechanism [26–29]. For example, when n is equal to 1, the oxidation reaction rate follows the linear law and the oxidation process is controlled by the reaction rate of oxygen and the substrate. When n is equal to 0.5, the oxidation reaction rate follows the parabolic law and the oxidation process is controlled by the diffusion of reactants in the oxide film. Based on the oxidation weight gain curves (Figure 1a), oxidation reaction indices were obtained through double logarithmic transformation, as shown in Figure 1b. However, considering the influencing factors of a lower oxidation weight gain and measurement deviation at 873 K, it was difficult to discuss the oxidation mechanism of TF550 alloy based only on the oxidation reaction index.

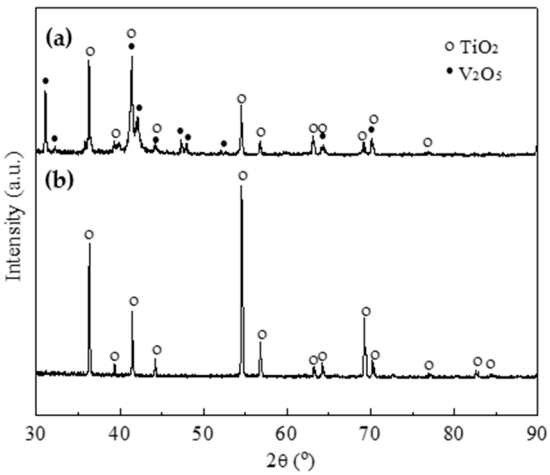

Figure 3. X-ray diffraction (XRD) profiles of TF550 alloy after oxidation at different temperatures for 100 h. (**a**) 873 K and (**b**) 1073 K.

Figure 4a shows the morphology of the oxide layer in TF550 alloy after oxidation at 873 K for 100 h, by SEM observation. The average thickness of the oxide layer was measured to be 7 μm. Figure 4b–f

show the EDS mapping of main elements of Ti, V, Cr, Si, and O. The concentration of O element in the oxide layer was higher than that of the substrate, while those of Ti and V elements in the oxide layer were lower. Combined with XRD results (Figure 3), the surface oxide layer consisted of TiO_2 and V_2O_5. Consequently, the oxidation process of TF550 alloy at 873 K was deduced to be controlled by the oxidation reaction at the interface between the substrate and oxide layer.

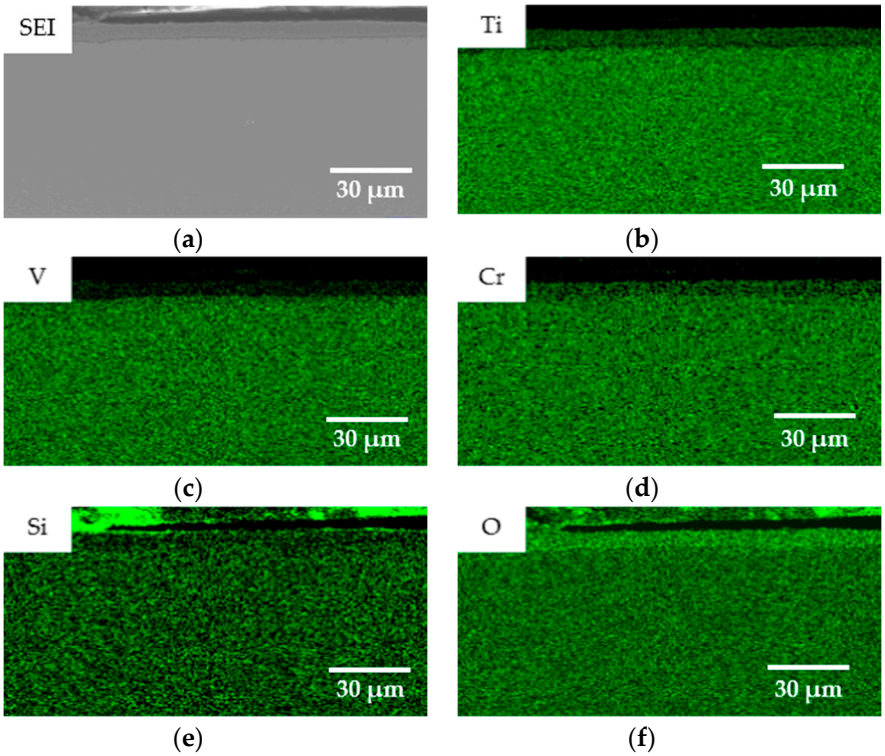

Figure 4. Scanning electron microscope (SEM) morphology and energy dispersive spectrometer (EDS) mapping of the oxide layer in TF550 alloy after oxidation at 873 K for 100 h. (**a**) Secondary electron image (SEI); (**b**) Ti element; (**c**) V element; (**d**) Cr element; (**e**) Si element; and (**f**) O element.

After oxidation at 1073 K for 100 h, the oxidation reaction index of TF550 alloy was analyzed to be 0.91, which was slightly larger than that (0.71) of Ti–6Al–4V alloy. The average thickness of the oxide layer as shown in Figure 5a was 460 μm after oxidation at 1073 K, which was much thicker than that of the oxide layer at 873 K. Based on the EDS mapping from Figure 5b–f, the Ti and O elements were clearly detected in the oxide layer, indicating that the oxide layer mainly consisted of TiO_2 combined with XRD results (Figure 3). The detected Si element on the top of Figures 4e and 5e was a residual polishing solution (SiO_2), which was considered to have no effect on the oxidation mechanism. Thus, the oxidation reaction rate at 1073 K followed the linear law and its oxidation process was controlled by the oxidation reaction at the interface between the substrate and oxide layer [26]. As shown in Figure 5c, the V element was clearly identified in the oxide layer, while the V_2O_5 was not detected by XRD as shown in Figure 3. Due to the low melting point of V_2O_5, they flowed into the crucible rather than adhered to the specimen, resulting in an absence of V_2O_5, which was in accordance with aforementioned occurrence of yellow matters in the crucible (Figure 2b). Furthermore, a positive concentration gradient of V occurred from the substrate to the surface due to the continuous consumption of V_2O_5 in the oxide layer, which accelerated the diffuse rate of V [30]. Consequently, V element was clearly detected in the oxide layer in terms of the EDS analysis.

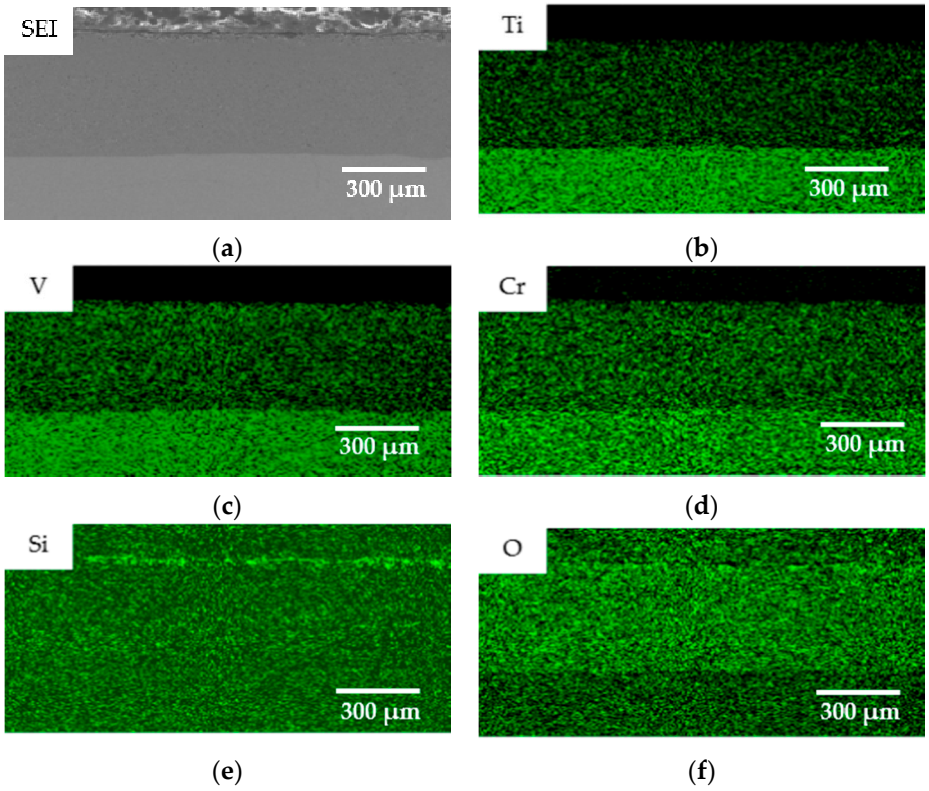

Figure 5. SEM morphology and EDS mapping of the oxide layer in TF550 alloy after oxidation at 1073 K for 100 h. (**a**) SEI; (**b**) Ti element; (**c**) V element; (**d**) Cr element; (**e**) Si element; and (**f**) O element.

Figure 6 shows the friction coefficients of TF550 alloy as a function of wearing time at 873 and 1073 K. The friction coefficient at 873 K was largely fluctuated with wearing time up to 10 min, and then reached a steady-state condition. Compared with 873 K, the friction coefficient at 1073 K became smaller, and its fluctuation became much weaker. The mean friction coefficient (f_m) at 873 and 1073 K, as listed in Table 1, were calculated to be 0.394 and 0.286, respectively. On the other hand, the volume wear rate of the disk (W_{sd}) at 873 K was obtained to be 2.21 $\times$ 10^{-13} m^3/Nm (Table 1), while it could not be measured at 1073 K because of the amount of oxides formed on the worn surface. For a comparison, the volume wear rate of the pin (W_{sp}) at 873 K was 0.197 $\times$ 10^{-13} m^3/Nm, which was smaller than that (0.566 $\times$ 10^{-13} m^3/Nm) of the pin at 1073 K (Table 1). Figure 7 shows the XRD profiles of worn surfaces for disks at different testing temperatures. Besides the β-phase, weak peaks of TiO_2 were detected on the worm surface at 873 K. Only peaks for both oxides, i.e., TiO_2 and V_2O_5, were present at 1073 K, while the peaks of the β-phase disappeared.

Table 1. Mean friction coefficient (f_m), volume wear rate of the disk (W_{sd}), and the pin (W_{sp}) in TF550 alloy after wearing at high temperatures of 873 and 1073 K.

Temperature (K)	f_m	W_{sd} (10^{-13}·m^3/Nm)	W_{sp} (10^{-13}·m^3/Nm)
873	0.394 ± 0.095	2.21 ± 0.35	0.197 ± 0.072
1073	0.286 ± 0.050	-	0.566 ± 0.039

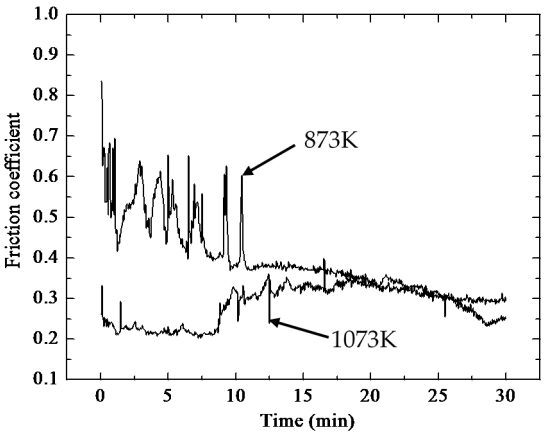

Figure 6. Friction coefficient curves of TF550 alloy as a function of wearing time at high temperatures of 873 and 1073 K.

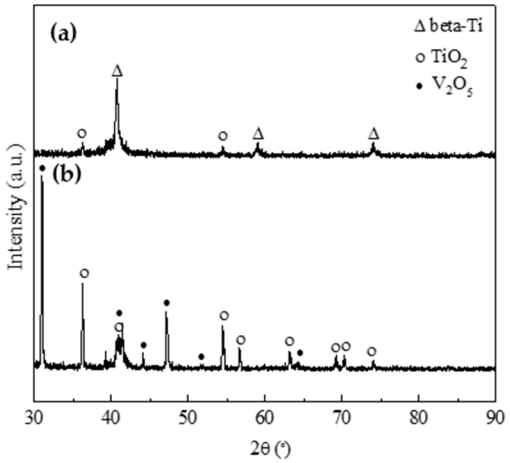

Figure 7. X-ray diffraction profiles of worn surfaces in TF550 alloy after wearing at high temperatures. (**a**) 873 K and (**b**) 1073 K.

Figure 8a shows the morphology of worn surfaces with a width of the wearing indent equal to about 1.2 mm at 873 K. Furrows indicated by arrows in Figure 8b were readily identified on the worn surface. Black smooth regions were also observed, which were regarded as tribo-layers containing the oxide of TiO_2 in terms of the EDS analysis (Figure 8c). In addition, some white particles consisting of not only metal debris but also the oxide of TiO_2 were confirmed by the EDS analysis as well (Figure 8d). Figure 9 shows the morphologies and compositions of worn surfaces at 1073 K. An average width of the wearing indent was 1.6 mm, and snowflake-like features were present on the worn surface (Figure 9a). The furrows were not observed and few black smooth regions appeared, as shown in Figure 9b; instead, a large amount of particles were present on the worn surface. The particles were further observed in Figure 9c and they were confirmed to be a mixture of the oxides of TiO_2 and V_2O_5, as shown in Figure 9d. Figure 10 shows the morphologies of the cross-section near the worn surfaces at 873 and 1073 K. The tribo-layer with an average thickness of 4 μm formed on the worn surface at 873 K (Figure 10a). However, this tribo-layer was not compact and it contained trace oxide of TiO_2, identified by EDS in Figure 10b. At 1073 K, the tribo-layer became thicker (7 μm) and more continuous, and it contacted with the matrix compactly in Figure 10c. This tribo-layer was identified as both TiO_2 and V_2O_5 oxides by EDS in Figure 10d.

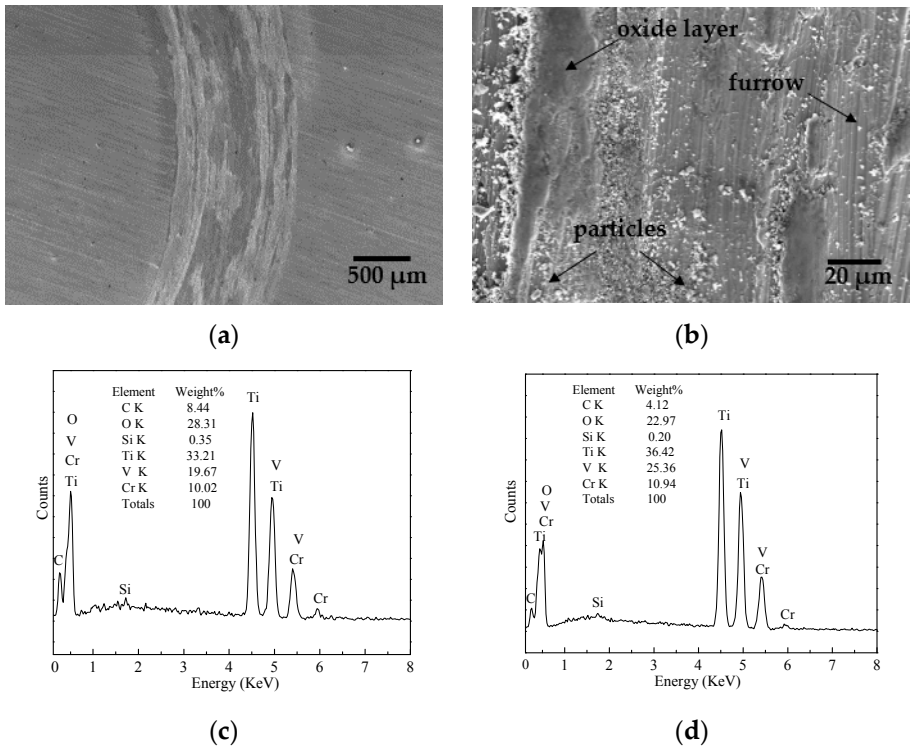

Figure 8. SEM morphologies and EDS spot-analyses of the worn surface in TF550 alloy after wearing at 873 K. (**a**) Low magnification SEI; (**b**) high magnification SEI; (**c**) compositions of the oxide layer region; and (**d**) compositions of the particles region.

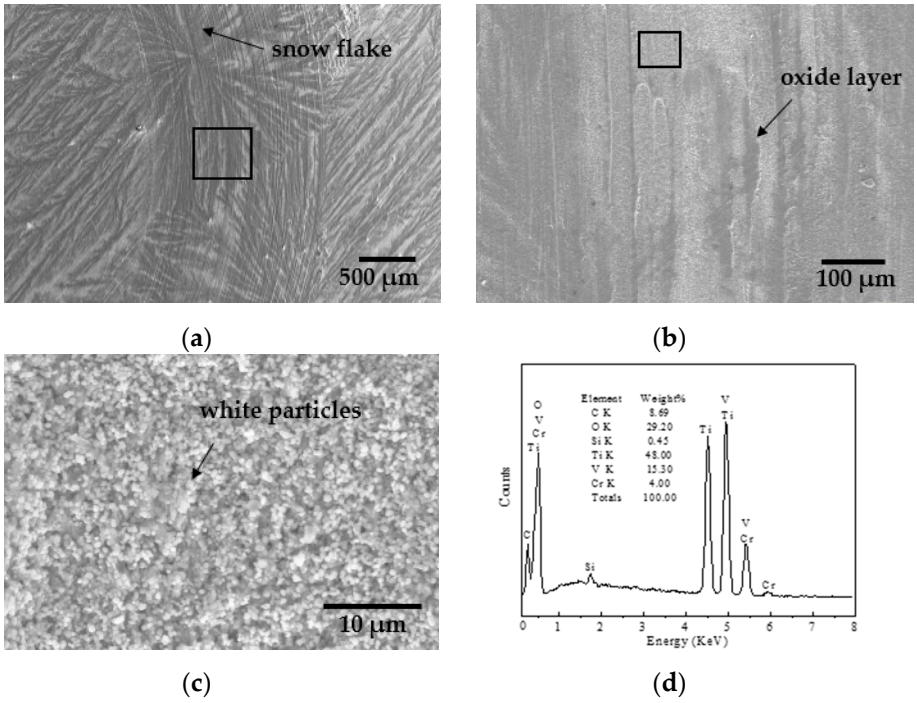

Figure 9. SEM morphologies and EDS spot-analysis of the worn surface in TF550 alloy after wearing at 1073 K. (**a**) Low magnification SEI; (**b**) high magnification SEI of area in black square in (**a**); (**c**) SEI of area in black square in (**b**); (**d**) compositions of the white particles region.

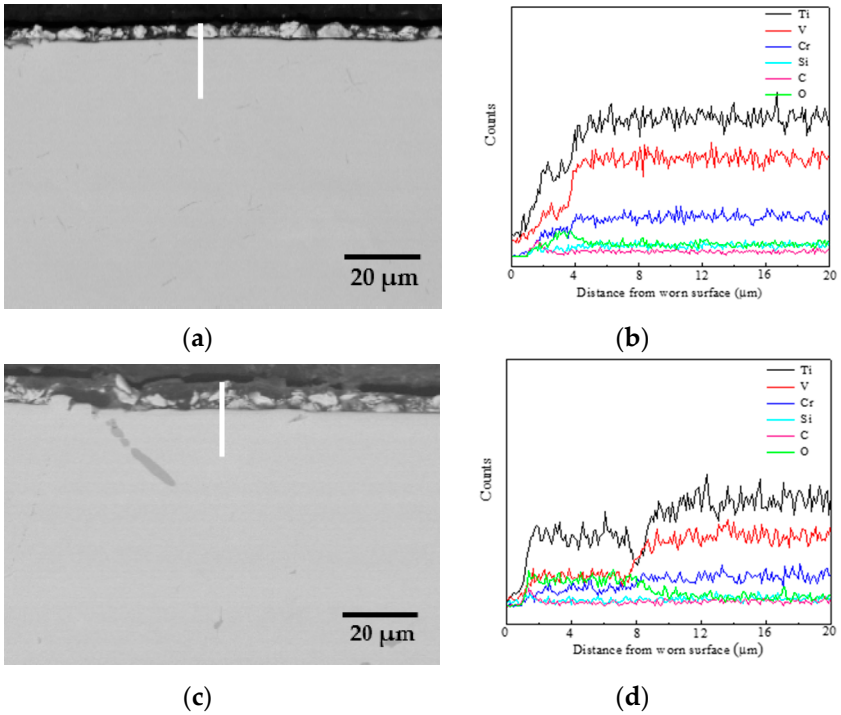

Figure 10. SEM cross-section morphologies and EDS line-analyses of the worn surface in TF550 alloy after wearing at high temperatures. (**a**) backscattered electron image (BEI) at 873 K; (**b**) compositions along the white line at 873 K; (**c**) BEI at 1073 K; and (**d**) compositions along the white line at 1073 K.

Based on the results of the friction coefficients, volume wear rates, and morphologies of worn surfaces, TF550 alloy presented different dry sliding wear behaviors at different testing temperatures. At 873 K, the tribo-oxide layer was not formed in the initial stage of dry sliding wear, and direct contact was not avoided completely, which resulted in a large friction coefficient. With an extension of wear time, a tribo-layer containing the oxide of TiO_2, i.e., black smooth regions formed, as shown in Figure 8b [31]. This tribo-oxide layer presented a partial protection from wearing for a decrease in the friction coefficient and its fluctuation. Some furrows appeared on the worn surface, while they were not covered with the tribo-oxide layer. Thus, the wear mechanism at 873 K was dominated by a combination of abrasive wear and oxidative wear. Amounts of oxides formed on the worn surface before the sliding test wear at 1073 K, because the temperature rose to the testing value in advance. The oxides formed before the sliding wear were loose, and thus were easily peeled off under the sliding in the initial period. Furthermore, V_2O_5 oxides could be melted during the sliding wear according to the oxidation morphology of TF550 alloy at 1073 K (Figure 2b). The molten V_2O_5 as a soft phase provided a lubricating effect, which led to a decrease in the friction coefficient, leading to a reduction of calorific value. Also, they filled defects between the hard phases, such as TiO_2 and metal debris, which could release the internal force between them, as shown in Figure 10c. Not only the loose oxides but also the molten V_2O_5 acted as a lubricant, leading to the absence of the running-in period and a relatively small friction coefficient during the wear process. The molten V_2O_5 flowed into the wear scratch and was subjected to solidification after wear testing, to exhibit the aforementioned snowflake-like features (Figure 9a), which was not in agreement with that of the single oxidation at 1073 K. In addition, the presence of amounts of oxides at relatively high temperatures made it difficult to measure the volume wear rate of the disk and resulted in an overestimated volume wear rate of the pin (Table 1). The furrows were not observed on the worn surface and amounts of oxide particles were present at 1073 K, indicating a typical feature of the oxidative wear mechanism.

4. Conclusions

In this study, the oxidation and wear characteristics of TF550 fireproof titanium alloy were investigated at high temperatures of 873 and 1073 K, and corresponding high temperature oxidation and wear mechanisms were also discussed. The main results are summarized as follows.

(1) The oxidation gain of TF550 alloy was much larger than that of Ti64 alloy, attributed the abundant addition of vanadium, which was regarded as a positive factor to improve the burn resistance. The oxidation weight gain of TF550 alloy after oxidation at 873 K for 100 h was much smaller than that at 1073 K for 100 h. The thin surface oxide film was identified as oxides of TiO_2 and V_2O_5 at 873 K, while the thick one was detected to be TiO_2 only at 1073 K. The oxidation reaction rate at 1073 K followed the linear law, indicating that the oxidation process of this alloy was mainly controlled by the oxidation reaction at the interface between the substrate and oxide layer.

(2) The friction coefficient at 873 K was larger than that at 1073 K, while the volume wear rate at 1073 K was larger because a large amount of oxides formed on the worn surface. The TiO_2 oxide was detected on the worn surface at 873 K, and both oxides of TiO_2 and V_2O_5 were present at 1073 K.

(3) The presence of furrows and a tribo-oxide layer at 873 K indicated that the wear mechanism was dominated by a combination of abrasive wear and oxidative wear. The continuous tribo-oxide layer was present at 1073 K, indicating that the wear mechanism was dominated by oxidative wear.

Acknowledgments: This work was financially supported by the National Natural Science Foundation of China, China (Grants Nos. 51471155 and 51471040). The authors would like to thank Jie Zhao and Wei Zhang of Dalian University of Technology for their assistance.

Author Contributions: Xiaohua Min and Guangbao Mi conceived and designed the experiments; Kai Yao and Pengfei Bai performed the experiments, analyzed the data and wrote the paper; Congqian Cheng contributed some analysis tools.

Conflicts of Interest: The authors declare no conflict of interest.

References

1. Banerjee, D.; Williams, J.C. Perspectives on Titanium Science and Technology. *Acta Mater.* **2013**, *61*, 844–879. [CrossRef]
2. Min, X.H.; Tsuzaki, K.; Emura, S.; Tsuchiya, K. Heterogeneous twin formation and its effect on tensile properties in Ti–Mo based β titanium alloys. *Mater. Sci. Eng. A* **2012**, *554*, 53–60. [CrossRef]
3. Min, X.H.; Emura, S.; Zhang, L.; Tsuzaki, K.; Tsuchiya, K. Improvement of strength-ductility tradeoff in β titanium alloy through pre-strain induced twins combined with brittle ω phase. *Mater. Sci. Eng. A* **2015**, *646*, 279–287. [CrossRef]
4. Luo, Q.S.; Li, S.F.; Pei, H.P. Progress in titanium fire resistant technology for aero-engine. *J. Aerosp. Power* **2012**, *27*, 2763–2767.
5. Zhang, P.Z.; Xu, Z.; Zhang, G.H.; He, Z.Y. Surface plasma chromized burn-resistant titanium alloy. *Surf. Coat. Technol.* **2007**, *201*, 4884–4887. [CrossRef]
6. Lv, D.S.; Xu, J.H.; Ding, W.F.; Fu, Y.C.; Yang, C.Y.; Su, H.H. Tool wear in milling Ti40 burn-resistant titanium alloy using pneumatic mist jet impinging cooling. *J. Mater. Process. Technol.* **2016**, *229*, 641–650. [CrossRef]
7. Zhang, X.J.; Cao, Y.H.; Ren, B.Y.; Tsubaki, N. Improvement of high-temperature oxidation resistance of titanium-based alloy by sol-gel method. *J. Mater. Sci.* **2010**, *45*, 1622–1628. [CrossRef]
8. Wang, M.M.; Zhao, Y.Q.; Zhou, L.; Zhang, D. Study on creep behavior of Ti–V–Cr burn resistant alloys. *Mater. Lett.* **2004**, *58*, 3248–3252. [CrossRef]
9. Xin, S.W.; Zhao, Y.Q.; Zeng, W.D.; Wu, H. Research on thermal stability of Ti40 alloy at 550 °C. *Mater. Sci. Eng. A* **2008**, *477*, 372–378. [CrossRef]
10. Li, Y.G.; Blenkinsop, P.A.; Loretto, M.H.; Walkern, N.A. Structure and stability of precipitates in 500 °C exposed in Ti–25V–15Cr–*x*Al. *Acta Mater.* **1998**, *46*, 5777–5794. [CrossRef]
11. Seagle, S.R. The state of the USA titanium industry in 1995. *Mater. Sci. Eng. A* **1996**, *213*, 1–7. [CrossRef]

12. Chen, Y.N.; Huo, Y.Z.; Song, X.D.; Bi, Z.Z.; Gao, Y.; Zhao, Y.Q. Burn-resistant behavior and mechanism of Ti14 alloy. *Int. J. Miner. Metall. Mater.* **2016**, *23*, 215–221. [CrossRef]
13. Campo, K.N.; Lima, D.D.; Lopes, E.S.N.; Caram, R. On the selection of Ti–Cu alloys for thixoforming processes: Phase diagram and microstructural evaluation. *J. Mater. Sci.* **2015**, *50*, 8007–8017. [CrossRef]
14. Chen, Y.N.; Yang, W.Q.; Zhan, H.F.; Zhang, F.Y.; Huo, Y.Z.; Zhao, Y.Q.; Song, X.D.; Gu, Y.T. Tailorable burning behavior of Ti14 alloy by controlling semi-solid forging temperature. *Materials* **2016**, *9*, 697. [CrossRef]
15. Mi, G.B.; Huang, X.; Cao, J.X.; Wang, B.; Cao, C.X. Microstructure characteristics of burning products of Ti–V–Cr fireproof titanium alloy by frictional ignition. *Acta Phys. Sin.* **2016**, *65*, 1–10.
16. Cao, J.X.; Huang, X.; Mi, G.B.; Sha, A.X.; Wang, B. Research progress on application technique of Ti–V–Cr burn resistant titanium alloys. *J. Aeronaut. Mater.* **2014**, *34*, 92–97.
17. Mi, G.B.; Cao, C.X.; Huang, X.; Cao, J.X.; Wang, B.; Sui, N. Non-isothermal oxidation characteristic and fireproof property prediction of Ti–V–Cr type fireproof titanium alloy. *J. Mater. Eng.* **2016**, *44*, 1–10.
18. Molinari, A.; Straffelini, G.; Tesi, B.; Bacci, T. Dry sliding wear mechanisms of the Ti6Al4V alloy. *Wear* **1997**, *208*, 105–112. [CrossRef]
19. Cui, X.H.; Mao, Y.S.; Wei, M.X.; Wang, S.Q. Wear Characteristics of Ti–6Al–4V Alloy at 20–400 °C. *Tribol. Trans.* **2012**, *5*, 185–190. [CrossRef]
20. Sun, Q.C.; Hu, T.C.; Fan, H.Z.; Zhang, Y.S.; Hu, L.T. Dry sliding wear behavior of TC11 alloy at 500 °C: Influence oflaser surface texturing. *Tribol. Int.* **2015**, *92*, 136–145. [CrossRef]
21. Mao, Y.S.; Wang, L.; Chen, K.M.; Wang, S.Q.; Cui, X.H. Tribo-layer and its role in dry sliding wear of Ti–6Al–4V alloy. *Wear* **2013**, *297*, 1032–1039. [CrossRef]
22. Zeng, S.W.; Jiang, H.T.; Zhao, A.M. High Temperature Oxidation Behavior of TC4 Alloy. *Rare Met. Mater. Eng.* **2015**, *44*, 2812–2816.
23. Zeng, S.W.; Zhao, A.M.; Jiang, H.T.; Fan, X.; Duan, X.G.; Yan, X.Q. Cyclic Oxidation Behavior of the Ti–6Al–4V Alloy. *Oxid. Met.* **2014**, *81*, 467–476. [CrossRef]
24. Mendez, S.F.O.; Rodriguez, C.R.S.; Venegas, K.C.; Aquino, J.A.M.; Magana, F.E. Magnetism and decarburization-like diffusion process on V_2O_5-doped ZnO ceramics. *Ceram. Int.* **2015**, *41*, 6802–6806. [CrossRef]
25. Li, Y.; Bai, C.Y.; Deng, X.Y.; Li, J.B.; Jing, Y.N.; Liu, Z.M. Effect of V_2O_5 addition on the properties of reaction-bonded porous SiC ceramics. *Ceram. Int.* **2014**, *40*, 16581–16587. [CrossRef]
26. Birks, N.; Meier, G.H.; Pettit, F.S. *Introduction of Metal Oxidation at High Temperature*; Higher Education Press: Beijing, China, 2010; p. 43.
27. Tomasi, A.; Gialanella, S. Oxidation phenomena in a Ti_3Al base-alloy. *Therm. Acta* **1995**, *269*, 133–143. [CrossRef]
28. Frangini, S.; Mignone, A.; De Riccardis, F. Various aspects of the air oxidation behavior of a Ti6Al4V alloy at temperatures in the range 600–700 °C. *J. Mater. Sci.* **1994**, *29*, 714–720. [CrossRef]
29. Jia, W.J.; Zeng, W.D.; Zhang, X.M.; Zhou, Y.G.; Liu, J.R.; Wang, Q.J. Oxidation behavior and effect of oxidation on tensile properties of Ti60 alloy. *J. Mater. Sci.* **2011**, *46*, 1351–1358. [CrossRef]
30. Huang, X.; Cao, C.X.; Ma, J.M.; Wang, B.; Gao, Y. High temperature oxidation behavior of a fire-resistant titanium alloy. *Rare Met. Mater. Eng.* **1997**, *26*, 27–30.
31. Wang, L.; Zhang, Q.Y.; Li, X.X.; Cui, X.H.; Wang, S.Q. Dry Sliding Wear Behavior of Ti–6.5Al–3.5Mo–1.5Zr–0.3Si Alloy. *Metall. Mater. Trans. A* **2014**, *45A*, 2284–2296. [CrossRef]